

The effect of slip regime on fretting wear-induced stress evolution

J. Ding, S. B. Leen*, I. R. McColl

School of Mechanical, Material, Manufacturing Engineering and Management

University of Nottingham, UK

*Corresponding author. Tel.: 0044-0115-9513812; fax: 0044-0115-9513800; email address: s.leen@nottingham.ac.uk. Mail address: School of Mechanical, Material, Manufacturing Engineering and Management, University of Nottingham, NG7 2RD, UK

Abstract

A numerical approach to simulate fretting wear, based on a modified version of the Archard equation, is applied to a cylinder-on-flat fretting configuration for gross sliding and partial slip conditions. The evolution of contact geometry, surface contact variables, including, contact pressure and relative slip, and sub-surface stresses are predicted. Surface wear damage is predicted to have a significant effect on the near-surface tangential and shear stress distributions for both slip regimes, with significant differences between the partial slip and gross slip cases. The implications of these effects are discussed with respect to fatigue prediction, leading to new insight into experimentally observed effects of slip regime on crack initiation. The more detrimental effects of partial slip conditions, with respect to cracking risk, are demonstrated quantitatively. In addition, the results suggest an explanation for the observed variations in location of crack

initiation within the slip zone under partial slip conditions. The work establishes a basis for direct incorporation of the effect of slip amplitude on fretting fatigue life prediction.

Keywords: finite element analysis, frictional contact, fretting wear, fretting fatigue, subsurface stress, slip regime, slip amplitude

Notation

a	contact half-width
c	the half width of the stick zone
c^*	the half width of the stick zone at the extreme of $T(t)$
E	Young's modulus
h	total wear depth
H	hardness of the material
k	dimensional Archard wear coefficient
K	non-dimensional Archard wear coefficient
N_t	total number of wear cycles
p_0	maximum Hertzian contact pressure
$p(x)$	contact pressure as a function of x -position
P	applied normal load
R	radius of contacting surface
$s(x)$	contact slip during a quarter cycle as a function of x -position
S	total (accumulated) slip distance
t	time

$T(t)$	friction force at time t
T_{\max}	maximum friction force during one fretting cycle
V	total wear volume
x, y	rectangular co-ordinates
$\delta(t)$	applied displacement as a function of time
δ^*	applied stroke half-amplitude
μ	coefficient of friction
σ_x, σ_y	normal stresses on planes perpendicular to the x, y axes
τ_{xy}	shear stress in x - y plane
ν	Poisson's ratio
ω	maximum penetration depth used in ABAQUS contact algorithm

Introduction

Fretting commonly occurs when two contacting bodies experience oscillating shear tractions and small relative slip amplitudes typically in the range 5 to 100 μm . The resulting damage can be either wear or fatigue, depending on the imposed forces and displacement amplitude. A theoretical basis for fretting fatigue and fretting wear analyses was first addressed by Cattaneo [1] and independently by Mindlin [2], who provided an analytical elastic solution of surface and subsurface stress distributions for the case of two spheres under partial slip. Their results were extended to other loading scenarios and contact geometries by Mindlin and Deresiewicz [3], Deresiewicz [4], Hamilton and Goodman [5] and Hamilton [6]. More recently, Hills and Nowell [7] published a review of analytical and numerical solutions of this problem involving various plane and

axi-symmetric configurations.

There is no general agreement on the use of the above-mentioned solutions for the analysis of fretting fatigue and fretting wear, as wear may significantly modify the initial surface profiles and, therefore, the surface and subsurface stress distributions. Hills and Fellows [8] reported some considerations about changes of indenter shape under the partial slip situation. They suggested that, since wear on a Hertzian (i.e. cylindrical) indenter is small enough to have only a modest influence on the contact-stress state, the use of the initial contact geometry is justified for predicting fretting fatigue. For the case of full sliding, Dundurs and Comninou [9] deduced a closed-form solution for the worn shape of an elastically rigid slider, assuming the high spots are worn until a uniform pressure exists. However, it should be pointed out that these two works only considered the change of indenter profile, not both indenter and counter-body profiles.

With the rapid development of finite element (FE) analysis for non-linear problems including contact mechanics, it is possible to tackle contact-based wear modelling. In 1994, Johansson [10] proposed an FE algorithm to simulate evolution of the contacting surface profiles and contact pressure, as induced by fretting wear. The present authors [11] recently implemented an FE-based wear simulation method, using a commercial FE code, and compared the predicted results against experimental wear measurements. This paper investigates the evolution of subsurface stress fields due to material removal by fretting wear, under both partial slip and gross slip regimes, using the latter wear simulation tool.

Formulation of analytical solution

The cylinder-on-flat configuration is widely employed in the study of fretting, since the solution for the initial stress, strain and slip fields is well known. A brief summary of relevant theories and solutions is given in this section.

Consider the fretting contact depicted schematically in Figure 1. The indenter is subject to a normal load P and an alternating tangential force $T(t)$ of amplitude T_{\max} , each per unit length of contact. If the two bodies have the same elastic modulus E , the deformations of their surfaces conform exactly to each other. The shape and size of the contact area are then determined by the profiles of the two surfaces and the normal load P , independent of the tangential force $T(t)$ [12]. The contact pressure $p(x)$ is given by the Hertzian solution [12]:

$$p(x) = p_0 \sqrt{1 - \frac{x^2}{a^2}} \quad (1)$$

The contact half-width a and the maximum contact pressure p_0 are given by:

$$a = \left(\frac{4PR}{\pi E^*} \right)^{\frac{1}{2}} \quad (2)$$

$$p_0 = \left(\frac{PE^*}{\pi R} \right)^{\frac{1}{2}} \quad (3)$$

where:

$$E^* = \left(\frac{1-\nu_1^2}{E_1} + \frac{1-\nu_2^2}{E_2} \right)^{-1} \quad (4)$$

$$R = \left(\frac{1}{R_1} + \frac{1}{R_2} \right)^{-1} \quad (5)$$

Subscripts 1 and 2 correspond to the contacting bodies and R represents the principal radius of curvature.

With the introduction of the tangential force $T(t)$, relative slip occurs between the two contact surfaces. In gross slip situations, the maximum tangential force, T_{max} , is equal to the limiting friction force, i.e. μP , where μ is the coefficient of friction. Under this instantaneous condition, the shear traction is given by:

$$q(x) / \mu p_0 = -\sqrt{1 - (x/a)^2} \quad (6)$$

If T_{max} is less than μP , partial slip occurs and a central stick zone of half-width c can be developed with a partial slip zone occurring at the edge, $c \leq |x| \leq a$. The shear traction distribution corresponding to the extremes of $T(t)$ can be described by Mindlin theory as:

$$q(x) = \mu p_0 \left\{ (a^2 - x^2)^{1/2} - (c^{*2} - x^2)^{1/2} \right\} / a \quad (7)$$

where c^* is the instantaneous half-width of the stick zone, and is given by:

$$\frac{c^*}{a} = \sqrt{1 - \frac{T_{max}}{\mu P}} \quad (8)$$

Details on the variation of the shear traction within one fretting cycle can be found in [13]. The stress components for gross slip can be deduced by superposition of the stresses due to the normal traction (pressure) $p(x)$ and the tangential traction $q(x)$. The explicit formulations were given by Smith & Liu [14] and Sackfield & Hills [15]. The stress fields for partial slip can be obtained by superimposing the stresses due to three

elliptical distributions, corresponding to (i) the normal traction distribution $p(x)$ over $|x| \leq a$, (ii) the shear traction distribution $\mu p(x)$ over $|x| \leq a$ and (iii) an additional shear traction distribution of magnitude $-\mu p(x/c)c/a$ over $|x| \leq c$ [7].

Finite element analysis

The general purpose, non-linear FE code, ABAQUS [16] is used to calculate the surface and subsurface stress distributions before and after wear. The finite element model is shown in Figure 2. The radius of the cylinder is 6 mm. Detailed attention has been given to the development of this finite element model, due to the difficulties associated with frictional contact modelling of deformable bodies [16] and a more detailed description of this development is given in [17]. However, some of the more important aspects are mentioned here. The predicted surface traction distributions and sub-surface normal and shear stresses have been validated for the unworn case [11,17] against the corresponding Hertzian results [12]. The mesh (element size) in the contact area is very fine (about 10 μm) to capture the complicated variations of surface and sub-surface stresses and relative slip. The transition from coarse mesh to fine mesh is achieved via multi-point constraints (MPCs). Two-dimensional, four-node, plane strain (linear) elements are employed throughout, as recommended for frictional contact problems [16]; second order elements can give fluctuating pressure distributions. The contact surface interaction is defined via the contact pair approach of ABAQUS, which uses a master-slave arrangement to enforce the non-penetration contact constraint. The use of matching slave and master surface meshes is well established to be critical to reliable surface traction results. During the iterative contact solution procedure, the nodes on the slave surface are

permitted to penetrate the master surface by a user-controlled maximum penetration depth ω . In this study the cylindrical surface was chosen as the slave contact surface and the recommended [16] ω value of approximately 5 μm , i.e. half the characteristic element dimension, was employed. An unsatisfactory value for ω would give rise to difficulties in achieving convergence or fluctuating surface tractions [16], neither of which occurred in the present context, either for the unworn or worn cases; the issue of instabilities in the wear simulation results has been discussed in detail in [11]. The wear simulation algorithm [11] modifies the contact geometry in such a way as to maintain matching meshes throughout the total wear simulation, thus ensuring smooth surface and sub-surface stress distributions. In addition, the through-depth dimensions of the surface elements are maintained approximately constant by ‘shunting’ down the sub-surface rows of nodes, as the surface nodes are moved, so as to maintain essentially the same surface element and sub-surface element depths. This ensures that implementation of the wear does not affect adversely the element sizes or shapes, and that the worn meshes give equivalent quality results to the validated unworn results. The basic Coulomb friction model, implemented using isotropic friction in ABAQUS, is employed, with the frictional contact conditions introduced via the Lagrange multiplier approach, for both normal and tangential loading. This enforces exact sticking (zero slip) constraints between the bodies when the equivalent shear stress is less than the critical shear stress. The alternative approach is the more-approximate penalty method that permits an allowable elastic slip for ease of convergence. Coefficient of friction μ is taken as 0.6 from the fretting tests reported in [11], for the configuration modelled here.

The elastic modulus and Poisson’s ratio of both the cylinder and flat are taken as

200 GPa and 0.3, respectively. Linear constraint equations are employed to ensure uniform vertical displacement of the nodes on the top surface of the cylinder. To simulate the fretting contact, a y direction normal load is applied to the top surface, and then a periodic x direction displacement $\delta(t)$ of amplitude δ^* is imposed on Point F (see Figure 2), introducing an oscillatory tangential friction force $T(t)$ on the contacting surfaces. The bottom of the flat substrate is restrained from movement in the x and y directions. In this paper two different loading cases are studied (see Table 1), corresponding to gross slip and partial slip situations, respectively.

Wear simulation method

A commonly used model for sliding wear damage is Archard's equation [18]:

$$\frac{V}{S} = K \frac{P}{H} \quad (9)$$

where V is the wear volume, S is the sliding distance, K is the wear coefficient, P is the normal load and H is the hardness of the material. For a given point on one of the contacting surfaces, Equation (9) can be expressed as:

$$\frac{h}{S} = kp \quad (10)$$

where h is the wear depth (m), k is the dimensional wear coefficient (MPa^{-1}) and p is the contact pressure (MPa). The differential formulation of Equation (10) is:

$$\frac{dh}{dS} = kp \quad (11)$$

Based on Equation (11), a numerical approach has been developed to simulate

fretting wear. The approach is shown schematically in Figure 3. Specifically, for a given contact geometry, the initial distributions of contact pressure and relative slip between the contact surfaces are calculated by the finite element method. With this information, the nodal wear depth for one increment of wear cycles (ΔN) is computed, permitting the modified geometry of the FE model to be determined. Wear simulation is achieved by repeating this procedure incrementally. Further detail can be found in [11]. It should be noted that the effect of debris is neglected in the simulation described here.

Evolution of stresses due to wear

In order to assess the effect of fretting wear on the two-dimensional contact stress distributions, the wear simulation approach has been applied for the two load cases of Table 1, with an assumed dimensional wear coefficient of $1.0 \times 10^{-7} \text{ MPa}^{-1}$. This value is representative of a nitrided CrMoV high strength steel, up to 18,000 fretting wear cycles [11]. Figure 4 shows the contact surface profiles versus numbers of fretting wear cycles for gross slip (Case 1). Note that the horizontal and vertical positions refer, respectively, to the x and y coordinates of Figure 2, and that different scales are used for the horizontal and vertical axes. As fretting-wear proceeds, the contact surface profiles are modified, with the flat surface developing a dished profile; the contact tends towards conforming.

Figure 5a shows the FE predicted contact pressure distribution $p(x)$ versus number of fretting cycles for gross slip (Case 1). These distributions correspond to the instant of zero tangential displacement during the displacement cycle. The FE predicted distribution at zero cycles overlays the Hertzian calculated distribution except for a very small

dip at $x = 0$. As fretting wear proceeds, the size of the contact region increases and the peak $p(x)$ is dramatically reduced. At 18000 cycles, the peak $p(x)$ is predicted to have reduced to less than 15% of its initial value, and the pressure distribution along the contact tends towards uniform. Figure 5b shows the evolution of the contact slip $s(x)$ corresponding to the $+\delta$ extreme of the fretting cycle (i.e. $+10 \mu\text{m}$ displacement). From the unworn situation (0 cycles) to 18,000 cycles, the magnitude of $s(x)$ is predicted to increase by less than $1 \mu\text{m}$, although the extent of slip clearly increases from about 0.2 mm to more than 0.95 mm width, due to the increased contact area. The increase in $s(x)$ at the centre of the contact complements the decrease in contact pressure.

Evolution of the contact surface profiles also gives rise to variations in the subsurface stresses. Figure 6 shows the distribution of subsurface normal stress σ_x and shear stress τ_{xy} at the $+\delta$ extreme, at a depth of 0.005mm below the flat surface, for 0 and 18000 wear cycles. The normal stress σ_x has an initial maximum tensile (positive) stress of 450MPa at the initial trailing edge (Point A). However, after 18,000 wear cycles it is replaced by a small compressive (negative) stress at Point A. In contrast, at the new trailing edge (Point B) σ_x is still tensile, although it again has a much-reduced value of 120MPa. It is expected that σ_x at Point B will go negative with further development of fretting wear.

Figure 7 shows the theoretical distributions of the initial shear stress τ_{xy} at a depth of 0.005mm due to normal loading, sliding tangential loading (with $\mu = 0.6$) and the combined loading case, based on Hertzian contact theory [12]. The FE-predicted τ_{xy} distribution for the unworn case of Figure 6b slightly under-predicts the peak stress and

slightly over-predicts the contact edge stresses relative to the theoretical combined loading distribution (Figure 7). These differences can be attributed to the assumptions of Hertzian theory, e.g. elastic half-spaces, which is not the case for the FE model. Under normal loading only, the theoretical shear stress is anti-symmetric about the $x = 0$ position, with peak values occurring at the contact edges; in contrast, the tangential load distribution is symmetric about the $x = 0$ position and always of the same sign. The combined loading gives rise to a rather sharp dip in shear stress at the $x = -a$ contact edge; the FE model predicts a similar but somewhat sharper dip. The FE distributions also slide in the direction of applied displacement (Figure 6b). With the increasing number of fretting wear cycles, the shear stress τ_{xy} in the central region of contact is seen to decrease significantly, while a local peak appears at the leading edge of the enlarged contact zone. This local peak, which moves to the $x = -a$ edge of contact with reversing displacement, i.e. $-\delta$, is attributed to the stress concentration associated with the interaction between the cylindrical surface and the increasingly sharp wear scar edge.

If the imposed displacement is small enough, e.g. $2.5\mu\text{m}$ of Case 2, slip only occurs at the edge of the contact region and the central zone remains in a stick condition. The magnitude of slip is much smaller than the imposed displacement. Using the same wear coefficient as in Case 1, the predicted development of the contact surface profiles for the partial slip conditions of Case 2 are illustrated in Figure 8. There is no wear predicted in the stick region due to the absence of slip. Slight wear occurs in the slip regions, resulting in an increased gap for the undeformed (i.e. unloaded) configuration in these regions.

Figure 9 shows the evolution of the contact pressure and contact slip for Case 2. Note again that the contact pressure corresponds to zero tangential displacement of the

displacement cycle, whilst the contact slip corresponds to the $+\delta$ extreme, i.e. $+2.5\mu\text{m}$ displacement. After 18,000 cycles, the central stick zone remains unchanged, but the outer slip zone width has increased by 0.03mm (Figure 9b). Thus, the total contact width increases by 20%, even for the partial slip situation. The initial $p(x)$ distribution (Figure 9a) is still consistent with the Hertz solution. However, after 18,000 wear cycles, $p(x)$ in the stick zone increases significantly, particularly at the slip-stick boundaries where sharp peaks develop. In contrast, $p(x)$ in the slip zones is reduced to negligible values, due to the increased gap caused by wear. The pressure distribution tends towards that of a sharp-cornered punch of width equal to the initial stick zone width. Figure 9b shows that the contact slip increases by more than 50%, but the absolute values are still small relative to the applied displacement of $2.5\mu\text{m}$.

The effect of wear on the σ_x and τ_{xy} subsurface stress distributions at the $+\delta$ extreme, at a depth of 0.005mm below the flat surface, for Case 2, is illustrated in Figure 10. After 18000 wear cycles the maximum tensile value of σ_x is increased from about 400 to 460 MPa and its position moved from the initial (Hertzian) contact trailing edge (Point C) to the stick-slip boundary (Point D). In addition, unlike for gross slip (Case 1), the high tensile stress extends completely across the slip zone from the initial contact trailing edge (Point C). There is a more dramatic change in τ_{xy} with wear. The maximum value of τ_{xy} increases from about 400 MPa, for the unworn case, to about 1200 MPa at 18000 cycles, and the location of this maximum moves from the edge of contact to the stick-slip interface (point E in Figure 10b). Following the trend of contact pressure, the worn shear stress distribution evolves to become like that of a sharp-cornered punch. Theoretical solutions for the sub-surface stress distributions under a

sharp-cornered punch for non-sliding normal and tangential loading has been presented previously [19]. The distributions of Figure 10a and 10b show similar trends. The worn normal stress σ_x distribution (Figure 10a) is the superposition of a symmetric compressive stress distribution, with sharp peaks at the contact edges, and an anti-symmetric stress distribution, again with peaks at the contact edges, compressive at the leading stick-slip interface and tensile at the trailing stick-slip interface for the $+\delta$ stroke position. The symmetric distribution is attributable to the normal load and the anti-symmetric distribution to the traction induced shear load. The predicted resultant σ_x distribution thus gives a damaging local tensile peak at the trailing stick-slip interface. The worn τ_{xy} distribution of Figure 10b is amenable to similar interpretation. In particular, under the stick condition the stress distribution due to the normal load is dominant over that due to the tangential load, and the contact pressure distribution of Figure 9a is expected to give sharp anti-symmetric peaks in the τ_{xy} distribution at the leading and trailing stick-slip interfaces, similar to that of Figure 7. The distribution is shifted upwards with the superposition of the tangential load, resulting in the sharp, damaging positive τ_{xy} peak at the leading edge and the correspondingly sharp, but smaller, negative peak at the trailing edge.

Discussion

The present work has compared, for a cylinder-on-flat fretting arrangement, the fretting wear-induced changes in contact width, contact pressure and relative slip, under gross slip and partial slip conditions (Figures 5 and 9). The contact width increases with increasing number of wear cycles, although the increase is limited for partial slip. This is

consistent with experimental results by Fellows *et al* [20], for partial slip conditions. They reported the fretting scar widths to be larger than predicted by Hertz theory, although they attributed this to the effects of surface roughness. The present work suggests that this difference may well be fretting wear induced. Under gross slip conditions, recent work by the authors [11] has shown reasonable agreement between the numerical predictions and experimental fretting scars.

Although a considerable number of studies into fretting fatigue and fretting wear have been reported in the literature, some aspects are still not sufficiently well understood to permit successful quantitative modelling. One such is the effect of slip amplitude on both fretting wear and fretting fatigue, and the interaction between the two. Vingsbo and Soderberg [21] have summarised the relationship between fatigue life and wear rate as a function of slip amplitude, as shown in Figure 11; the risk for both wear and fatigue in the partial slip regime is increased with increasing slip amplitude. In contrast, in the gross slip regime, although the wear rate continues to increase with increasing slip amplitude, fatigue damage is reduced significantly. A general and simple proposed explanation for this is that embryo cracks are worn away before they have a chance to grow in the gross slip situations [22]. However, this phenomenon is difficult to implement in life prediction methods, due to the requirement for modelling of the three interacting aspects of short crack growth, frictional contact and material removal. Another observation not satisfactorily explained is the location of fretting fatigue cracks in the partial slip regime. With respect to Hertzian type contacts, e.g. cylinder-on-flat or sphere-on-flat, cracks have been observed to develop at the contact edge [23], within the slip zone [24] or at the slip-stick boundaries [25].

Numerous attempts have been made to predict the phenomenon of partial slip fretting fatigue, employing both stress or strain based approaches, e.g. maximum principal stress criterion [26], and empirical parameters, e.g. the Ruiz empirical parameter [27]. One disadvantage of the former is that they do not explicitly include the effect of slip amplitude. The Ruiz parameter, $\sigma\tau\delta$, where σ is the tangential near-surface stress, τ is the surface tangential stress and δ is the relative slip, was an attempt to empirically include the effect of slip amplitude in relation to the prediction of crack initiation for dovetail contact geometries. The method predicted the location of crack initiation accurately and consistently for that particular geometry and material combination but to the authors knowledge has not been generalised to other geometry and material combinations, especially for life prediction. During the last decade, most effort has focussed on the process of crack initiation, since it is argued that the bulk of a component's life is determined not by growth but by the initiation process itself [7, 28]. It is particularly emphasized that since the stress and strain beneath the contact are cyclic in nature, any attempt to predict the nucleation of fatigue cracks due the influence of fretting must account for the varying stresses [20,28]. Recently, Araujo and Nowell [23] have discussed the possibility of at least two distinct modes of crack initiation and early growth, namely tensile-dominated and shear-dominated. Which mode occurs depends on strain amplitude, material type and stress state. Araujo and Nowell [23] also investigated multiaxial fatigue models and techniques that can be used to predict crack initiation location and the direction of early growth. Specifically, they employed an extended Smith-Watson-Topper (*SWT*) parameter [29], for cracks that grow in planes of high tensile strain, and the Fatemi-Socie (*FS*) parameter [30], for cracks that grow in the

planes of high shear strain. The *SWT* parameter is expressed as:

$$SWT = \sigma_{\max} \left(\frac{\Delta \varepsilon}{2} \right) \quad (12)$$

where $\Delta \varepsilon$ is the difference between the maximum and minimum strains perpendicular to the critical plane during the displacement cycle and σ_{\max} is the maximum value of the stress component perpendicular to that plane at any point in the cycle; this parameter is maximised with respect to orientation of the plane to obtain the critical plane for crack initiation. The *FS* parameter, which is also maximised to obtain the critical plane, is expressed as:

$$FS = \frac{\Delta \gamma}{2} \left(1 + \alpha \frac{\sigma_{\max}}{\sigma_y} \right) \quad (13)$$

where $\Delta \gamma$ is the difference between maximum and minimum values of shear strain experienced during the cycle, σ_{\max} is the maximum value of the stress component normal to the chosen plane, σ_y is the yield stress and α is a constant which approaches unity at long lives and is reduced at shorter lives. These two parameters are calculated based on the unworn contact geometry and suggest initiation locations for the cylinder-on-flat configuration at the contact edges. Similarly, other stress or strain based methods neglecting wear also predict the initiation location at the contact edges, although the Dang Van and McDiarmid criteria have predicted the region of possible crack initiation to extend across the slip zone [31].

The results of the present work are critical for improved understanding of the initiation of fretting induced cracks in the presence of wear. For gross slip (Case 1), σ_{\max}

for the unworn geometry is approximately equal to σ_x at the trailing edge, since the corresponding shear stress τ_{xy} instantaneously vanishes. However, due to wear-induced material removal, the trailing edge σ_x changes to compressive with a significantly reduced magnitude; meanwhile τ_{xy} at the same position increases from zero to 80 MPa (Figure 6). Under such a modified stress field both the *SWT* and *FS* parameters after 18,000 wear cycles are significantly reduced from their values at zero cycles, so that the predicted risk of either tensile or shear type cracking is likewise significantly reduced.

For partial slip (Case 2), the region of high tensile σ_x grows, due to material removal, from the initial trailing edge to cover the complete slip zone, including the stick-slip boundaries, while τ_{xy} increases markedly at the stick-slip boundaries (Figure 10) half a cycle later. Under such a stress field, the location of σ_{\max} is calculated to shift to the stick-slip boundaries with an increase in magnitude, while $\Delta\varepsilon$ also increases, leading to an increased *SWT* at 18,000 wear cycles relative to the zero cycle value. This suggests that, if a tensile-type crack initiates within the early stages of fretting, when wear is negligible, the initiation site will be at or close to the trailing edge, whereas, if it initiates after tens of thousands of cycles when wear is not negligible, the initiation site will move to the stick-slip boundaries. This conclusion is in agreement with that of Goryacheva *et al.* [32], who evaluated the stress evolution in partial-slip fretting conditions using an analytical method.

On the other hand, with the appearance of the peak shear stress τ_{xy} at the stick-slip boundaries after wear, $\Delta\gamma$ also increases significantly and so does the *FS* parameter, leading to a much higher risk of shear-type cracking at the stick-slip boundaries. Since

either tensile or shear nucleation is possible at the stick-slip boundaries, the initiation angle can be expected to vary with the crack type.

It is clear from the above that wear has an important influence on the fretting fatigue initiation location and life prediction, and this influence is dependent on slip regime. Furthermore, according to the material removal phenomena reported on here, it appears that although slip is widely observed to affect fretting fatigue life, it does not necessarily need to be an explicit parameter in fretting fatigue prediction criteria, as proposed by Ruiz. Thus fretting fatigue life prediction can still be based on stress or strain based multiaxial fatigue methods, e.g. *SWT*, *FS* or Dang Van parameters, but the evolution of these subsurface stresses and strains due to material removal needs to be incorporated. It is important to note that in experimental investigations of partial slip fretting fatigue, a constant or cyclic tensile bulk stress is generally applied to the plain fatigue specimen onto which the contact pads are clamped, with a (generally) fixed normal clamping load and cyclic tangential loads [20,23]. Although the present work is based on a fretting wear test, which does not include the substrate fatigue stress, it is anticipated that the substantial trends with respect to the evolution of sub-surface stresses and strains under partial and gross slip conditions and their effect on crack initiation and early growth would not be altered by this aspect.

The primary advantage of the present FE-based approach is its versatility with respect to complexity of geometry, material properties and loading conditions. This facilitates application to more realistic components such as high performance aeroengine spline couplings [33], where fretting wear and life prediction are important issues, and where systematic component testing is expensive and the application of simplified

laboratory approaches is not straightforward due to the complexity of loading history. The present work then represents the basis for a general fretting fatigue lifing methodology for such complex components. Current work is focussed on two aspects, the application of multiaxial fatigue lifing methods to the complex stress and strain loading histories associated with friction contact between the spline teeth [34], and application of the wear simulation method to the same component using FE-predicted complex contact conditions. Together, these two aspects will permit lifing prediction including the effects of slip amplitude.

The evolution of stress presented here is based on the sub-surface stresses at a depth of 0.005mm, corresponding to the first row of Gaussian integration points (element sampling points) below the surface of the flat. This is true even for the worn geometry due to the rows of sub-surface nodes being ‘shunted’ down as the surface nodes are moved, in such a way as to maintain the same surface element depth and similar sub-surface element depths. Although further mesh refinement would give stress predictions at smaller depths and lead presumably to slightly different stress predictions and consequently to different fatigue life predictions, it is unlikely that the trends predicted would be changed significantly, particularly since these trends corroborate experimental findings from fretting tests. An apparent dilemma nonetheless arises in relation to the most appropriate choice of sampling depth for prediction of crack initiation. This issue has been dealt with previously in terms of the determination of an ‘averaging volume’ for fatigue parameters, which is typically empirically determined via correlation with test data, and appears to have some relationship to grain sizes [23, 31]. This aspect of an ‘averaging volume’ would therefore need to be considered in the application of the

present techniques to the prediction of crack nucleation.

Finally, the effects of wear debris on the wear process and on the change of surface and subsurface stresses are not dealt with above, but merit some discussion. From the tribological point of view, contact becomes much more complex with the introduction of debris. Godet *et al* [35] have proposed a theoretical model to describe the third-body, i.e. wear debris, which can accommodate load and displacement via elasticity, rupture, shear and/or rolling. However, quantification of the effect of wear debris on fretting wear and fretting fatigue remains a significant challenge. The authors will report on this aspect in future work.

Conclusions

Fretting wear is a surface degradation process, but it has been shown in this paper to have an important impact on the near-surface stresses, which affect the initiation of fretting fatigue cracks. For the gross slip regime, the high wear rate leads to the contact edges moving rapidly outwards, leaving the material previously at the contact edges in a permanently compressive state, which prohibits fretting-fatigue crack initiation. This suggests an explanation for wear being the predominant feature in gross slip with growth of a fretting fatigue crack being much less likely. For the partial slip regime, wear, although comparatively smaller, increases the maximum tensile normal stress and shifts its location from the contact edges to the boundaries between the stick and slip zones. The risk of crack nucleation is therefore greater at the contact edges for small numbers of cycles and at the stick-slip boundaries for large numbers of cycles. In addition, the dramatic increase in the shear stress at the stick-slip boundaries increases the risk of

nucleation of shear type cracks.

Acknowledgements

The authors would like to thank Rolls-Royce plc for financial assistance, and Thomas R Hyde and Nina Banarjee of Rolls-Royce plc, for helpful discussions.

References

1. Cattaneo C. Sul contatto di due corpi elastici: distribuzione locale degli sforzi Rendiconti Dell' Accademia nazionale dei Lincei 1938; **27**(6): 342-348, 434-436, 474-478.
2. Mindlin RD. Compliance of elastic bodies in contact. Journal of Applied Mechanics 1949; **16**: 259-268.
3. Mindlin RD, Deresiewicz H. Elastic spheres in contact under varying oblique forces. Trans. ASME, Series E, Journal of Applied Mechanics 1953; **20**: 327-344.
4. Deresiewicz H. Contact of elastic spheres under an oscillating torsional couple. Trans. ASME, Series E, Journal of Applied Mechanics 1954; **21**: 52-56.
5. Hamilton GM, Goodman LE. The stress field created by a circular sliding contact. Trans. ASME, Series E, Journal of Applied Mechanics 1966; **33**: 371-376.
6. Hamilton GM. Explicit equations for the stress beneath a sliding spherical contact. Proceedings of the Institution of Mechanical Engineers, Part C: Mechanical Engineering Science 1983; **197**: 53-59
7. Hills DA, Nowell D. *Mechanics of fretting fatigue*, Kluwer Academic Publishers, 1994.

8. Hills DA, Fellows LJ. Some observations on contact problems involving fretting in the presence of wear. *Wear* 1999; **231**(2): 319-324.
9. Dundurs J, Comninou M. Shape of a worn slider. *Wear* 1980; **62**: 419-424.
10. Johansson L. Numerical simulation of contact pressure evolution in fretting. *Journal of Tribology* 1994; **116**(2): 247-254.
11. McColl IR, Ding J, Leen SB. Finite element simulation and experimental validation of fretting wear. submitted to *Wear*.
12. Johnson KL. Contact mechanics. Cambridge University Press, Cambridge, 1985.
13. Maouche N, Maitournam MH, Dang Van K. On a new method of evaluation of the inelastic state due to moving contacts. *Wear* 1997; **203-204**: 139-147.
14. Smith JO, Liu CK. Stresses due to tangential and normal loads on an elastic solid. *Tran. ASEM, Series E, Journal of Applied Mechanics* 1953; **20**: 157-166.
15. Sackfield A, Hills DA. Some useful results in the classical Hertz contact problem. *Journal of Strain Analysis for Engineering Design* 1983; **18**(2): 101-105.
16. ABAQUS User's and Theory Manuals, Version 5.8, HKS Inc., Rhode Is., US, 1998.
17. Ding K. Modelling of fretting wear. PhD Thesis, University of Nottingham, UK, January, 2003.
18. Archard JF. Contact and rubbing of flat surfaces. *Journal of Applied Physics* 1953; **24**: 981-988.
19. Switek W. Early stage crack propagation in fretting fatigue. *Mechanics of Materials* 1984; **3**(3): 257-267.

20. Fellows LJ, Nowell D, Hills DA. On the initiation of fretting fatigue cracks. *Wear* 1997; **205**(1-2): 120-129.
21. Vingsbo O, Soderberg D. On fretting maps. *Wear* 1988; **126**(2): 131-147.
22. Waterhouse RB. Fretting wear. *ASM handbook, Volume 18, Friction, Lubrication, and Wear Technology* 1992, ASM International, 242-256.
23. Araujo JA, Nowell D. The effect of rapidly varying contact stress fields on fretting fatigue. *International Journal of Fatigue* 2002; **24**(7): 763-775.
24. Kuno M, Waterhouse RB, Nowell D, Hills D A. Initiation and growth of fretting fatigue cracks in the partial slip regime. *Fatigue and Fracture of Engineering Materials and Structures* 1989; **12**(5) 387-398.
25. Lamacq V, Dubourg MC, Vincent L. Crack path prediction under fretting fatigue - a theoretical and experimental approach. *Journal of Tribology* 1996; **118**: 711-720.
26. Nishioka K, Hirakawa K. Fundamental investigations of fretting fatigue, Part 5, Effect of relative slip amplitude. *Bulletin of JSME* 1969; **12**: 692-697.
27. Ruiz C, Boddington PHB, Chen K C. An investigation of fatigue and fretting in a dovetail joint. *Experimental Mechanics* 1984; **24**(3): 208-217.
28. Szolwinski MP, Farris TN. Mechanics of fretting fatigue crack formation. *Wear* 1996; **198**(1-2): 93-107.
29. Socie DF. Multiaxial fatigue damage model. *Journal of Engineering Materials and Technology* 1987; **109**(4): 293-298.

30. Fatemi A, Socie DF. Critical plane approach to multiaxial fatigue damage including out-of-phase loading. *Fatigue and Fracture of Engineering Materials and Structures* 1988; **11**(3): 149-165
31. Fouvry S, Elleuch K, Simeon G. Prediction of crack nucleation under partial slip fretting conditions. *Journal of Strain Analysis for Engineering Design* 2002; **37**(6): 549-564.
32. Goryacheva IG, Rajeev PT, Farris T N. Wear in partial slip contact. *Journal of Tribology* 2001; **123**: 848-856.
33. Leen SB, Hyde TH, Ratsimba CHH, Williams EJ, McColl I R. An investigation of the fatigue and fretting performance of a representative aero-engine spline coupling. *Journal of Strain Analysis for Engineering Design* 2002; **37**(6): 565-583.
34. Leen SB, Richardson IJ, McColl IR, Williams EJ, Hyde TR. Macroscopic fretting variables in a splined coupling under combined torque and axial load. *Journal of Strain Analysis for Engineering Design* 2001; **36**(5): 481-497.
35. Godet M, Berthier Y, Lancaster J, Vincent L, Wear Modelling: using fundamental understanding or practical experience. *Wear* 1991; **149**(1-2): 325-340.

Table 1. Parameters for fretting cases studied

Case	Normal load (N)	Peak-to-peak stroke amplitude (μm)
1	1200	± 10
2	1200	± 2.5

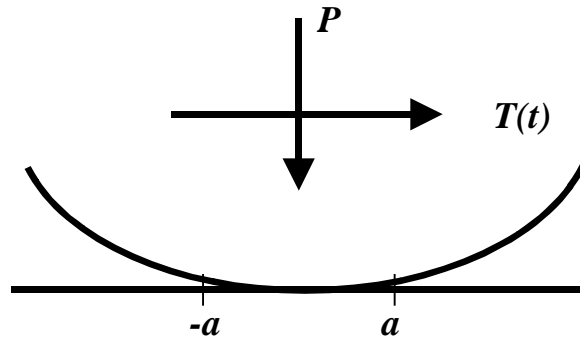


Figure 1. Fretting contact

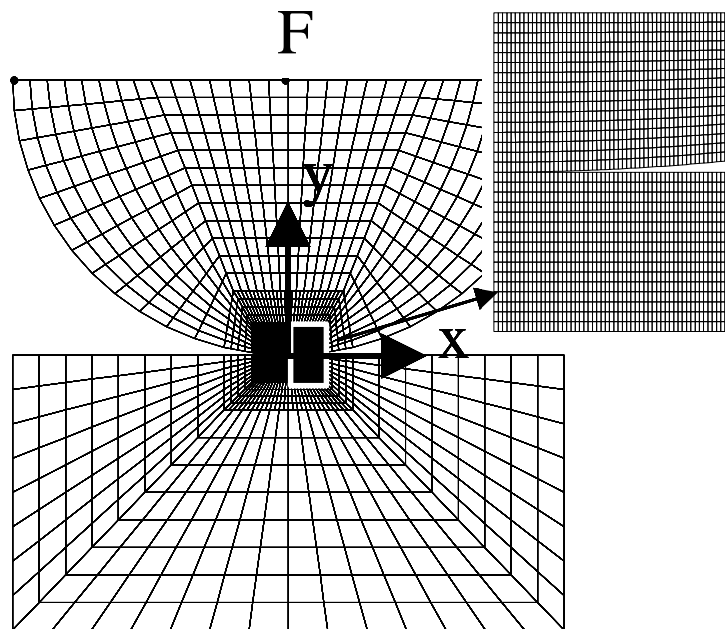


Figure 2. Finite element model of cylinder-on-flat configuration (note: x is horizontal position and y is vertical position in subsequent figures)

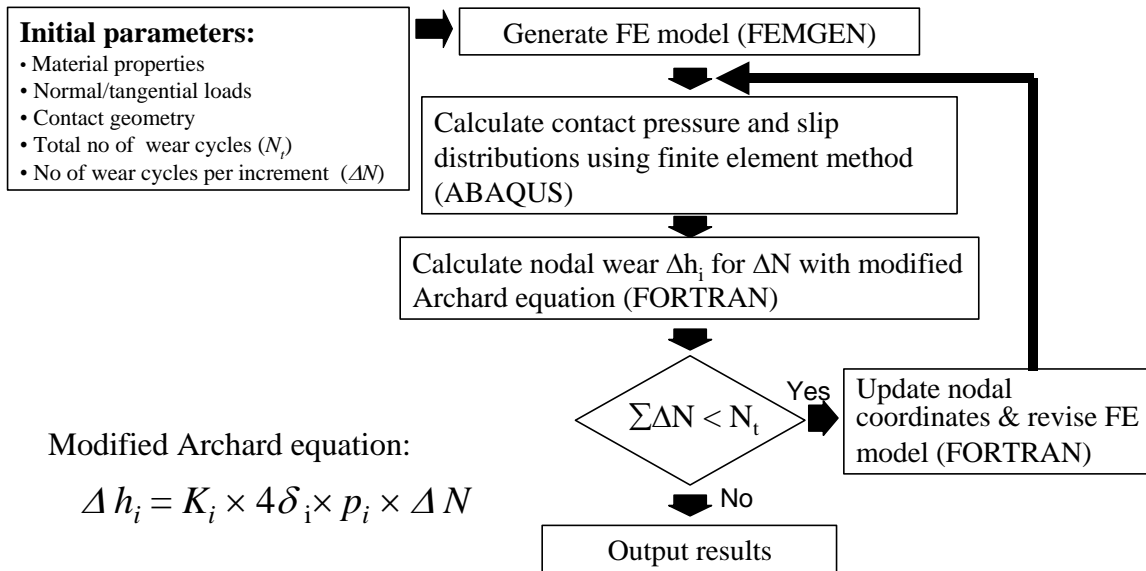
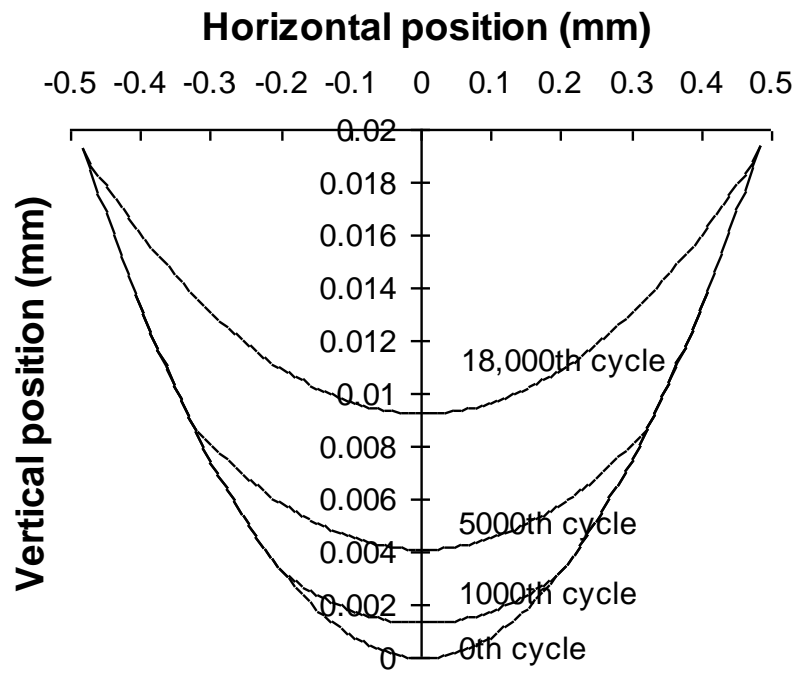
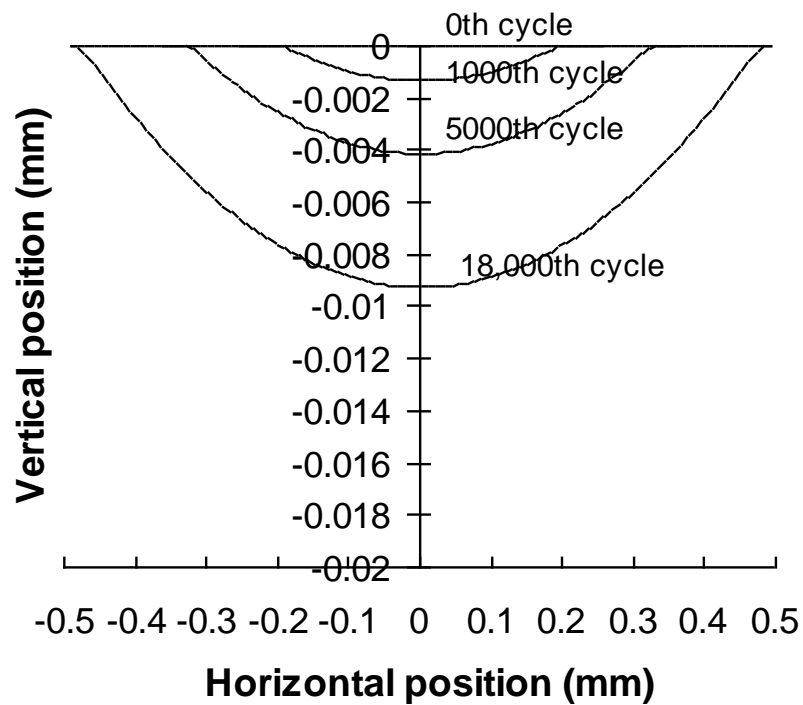


Figure 3. Schematic fretting wear simulation

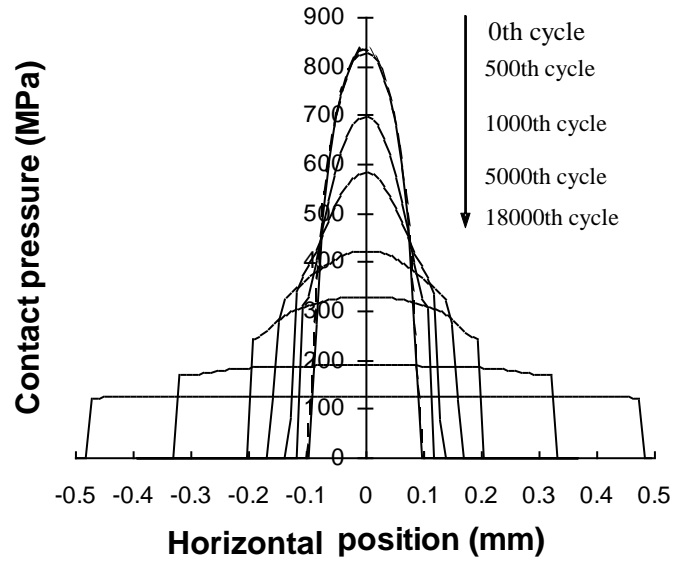


(a)

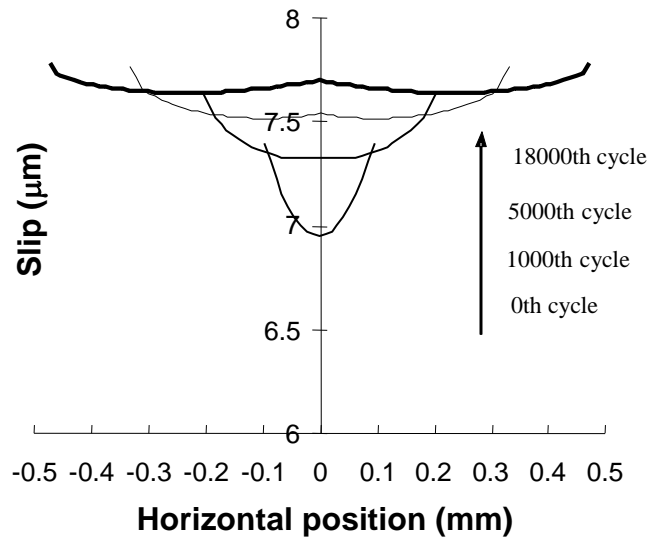


(b)

Figure 4. Surface profiles versus number of fretting wear cycles for Case 1 (gross slip): (a) cylindrical specimen and (b) flat specimen

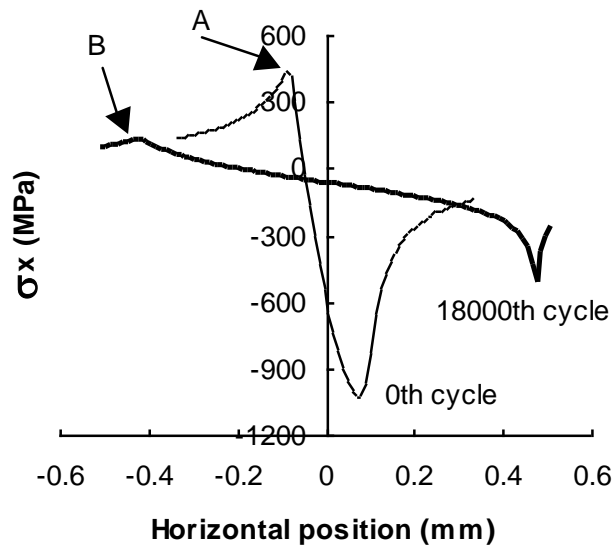


(a)

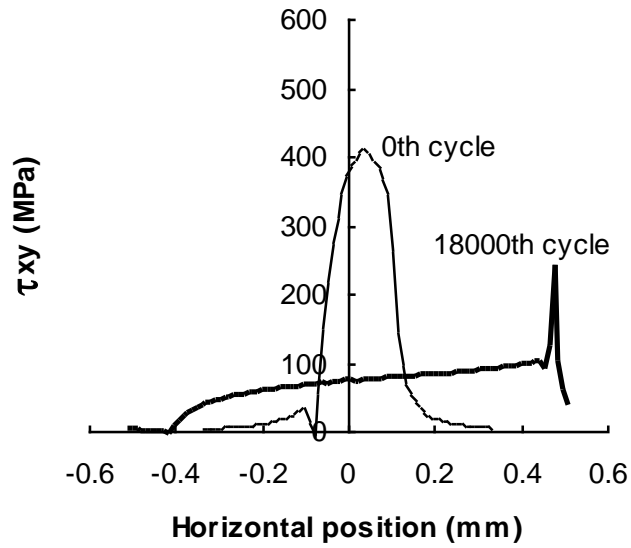


(b)

Figure 5. (a) Contact pressure and (b) relative slip versus number of fretting wear cycles for Case 1 (gross slip)



(a)



(b)

Figure 6. Subsurface stresses for the 0th and 18000th fretting wear cycles for Case 1 (gross slip): (a) normal stress σ_x and (b) shear stress τ_{xy}

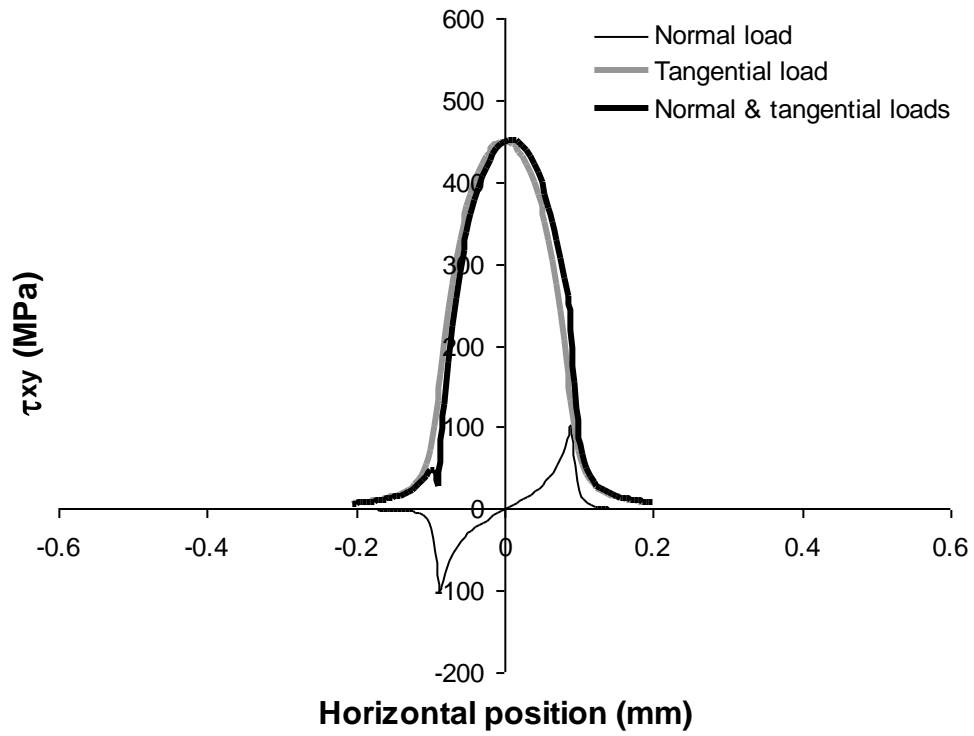
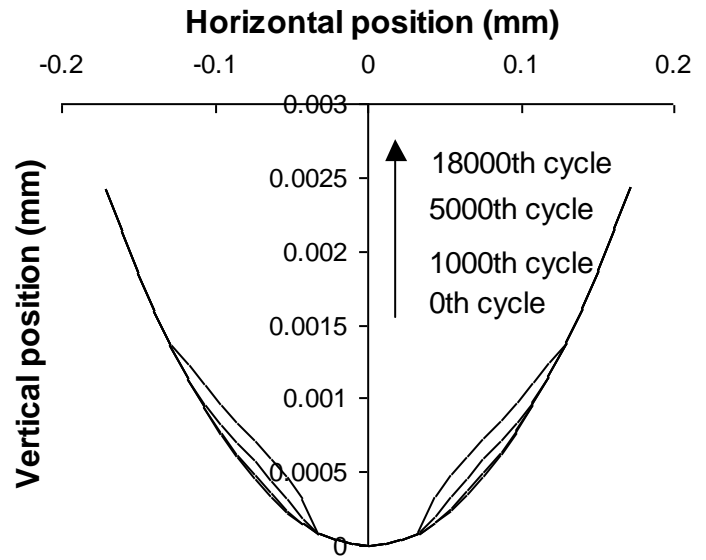
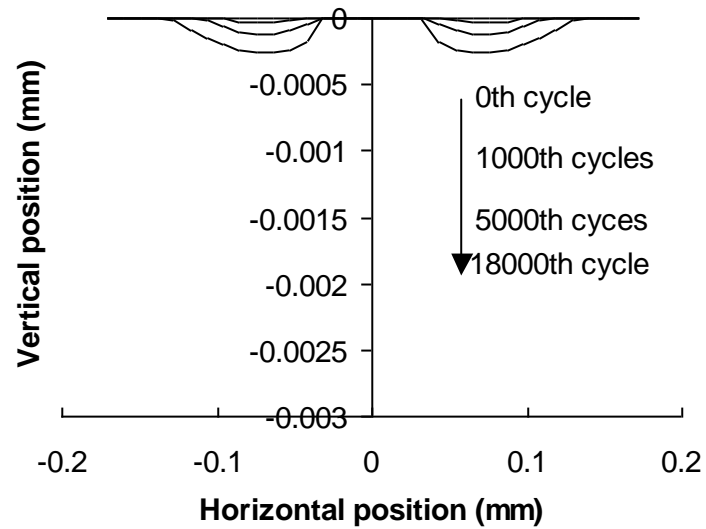


Figure 7. Hertzian predicted sub-surface τ_{xy} shear stress distributions at $y = -0.005$ mm for normal load only, sliding tangential load only ($\mu = 0.6$) and combined normal and tangential loading [12]

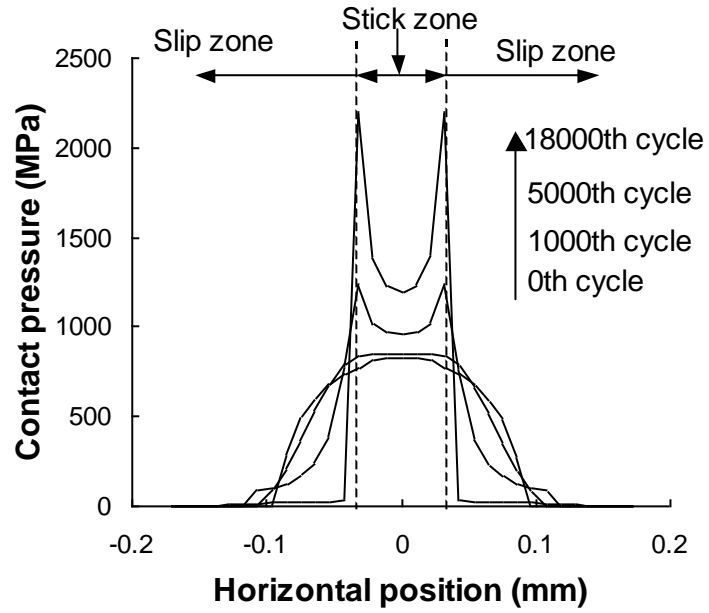


(a)

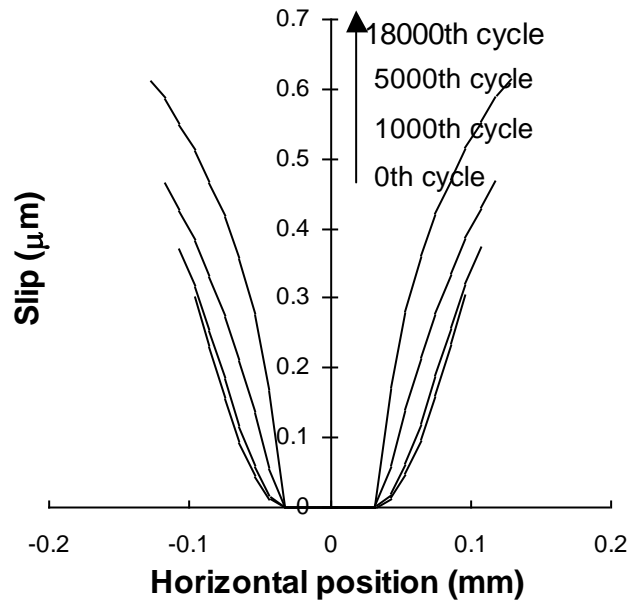


(b)

Figure 8. Surface profiles versus number of fretting wear cycles for Case 2 (partial slip): (a) cylindrical specimen and (b) flat specimen

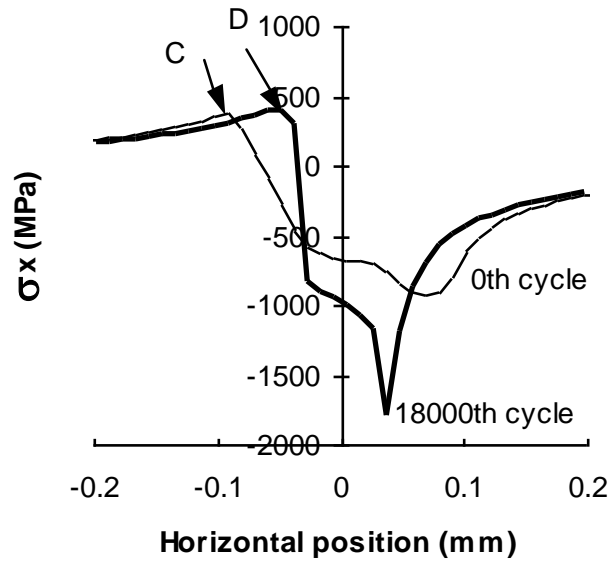


(a)

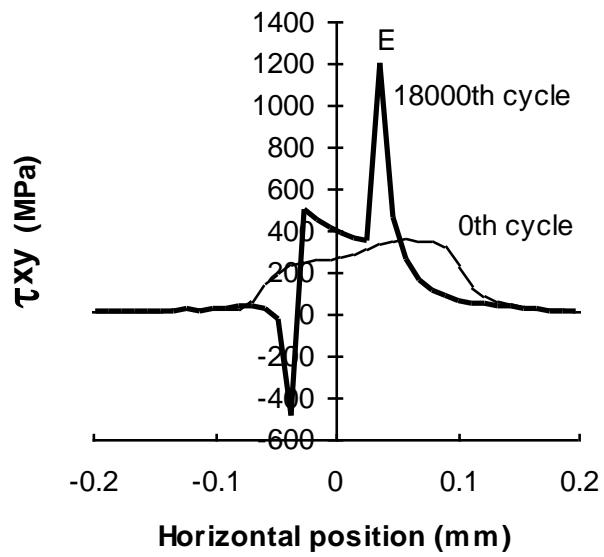


(b)

Figure 9. (a) Contact pressure and (b) relative slip versus number of fretting wear cycles for Case 2 (partial slip)



(a)



(b)

Figure 10. Subsurface stresses for the 0th and 18000th fretting wear cycles for Case 2 (partial slip): (a) normal stress σ_x and (b) shear stress τ_{xy}

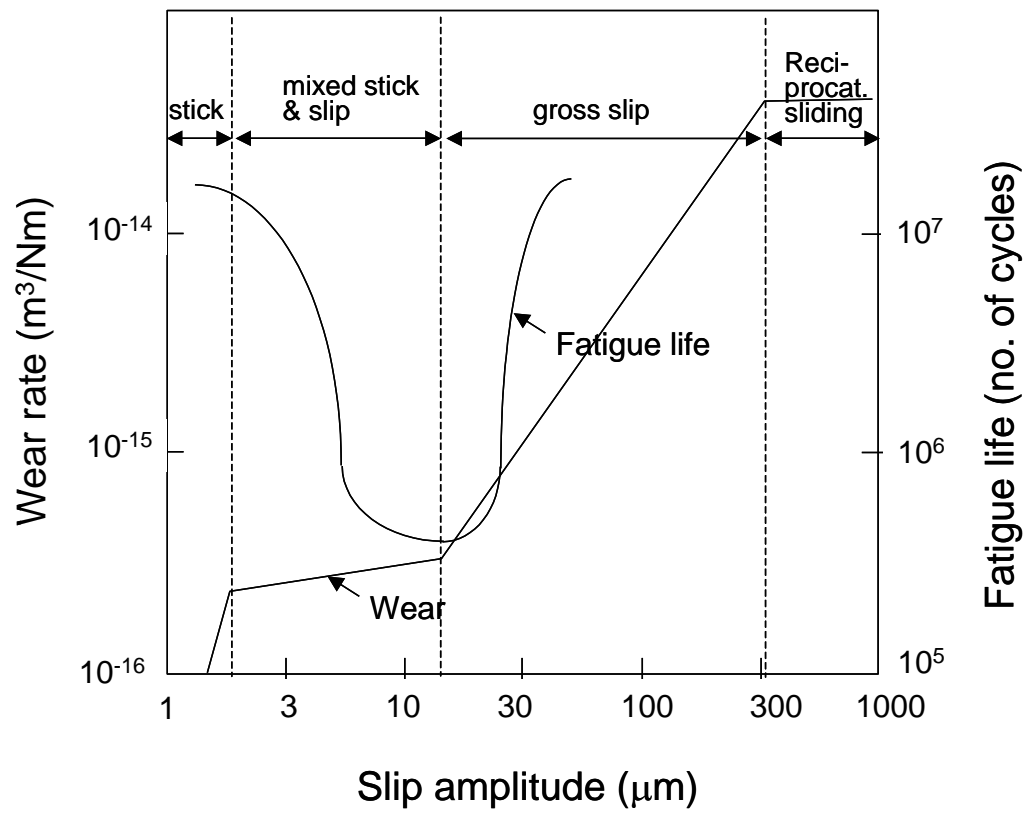


Figure 11. Typical relationship between fatigue life and wear rate as a function of slip amplitude, after Vingsbo and Soderberg [21]